Journal of Modern Optics
Vol. 58, Nos. 3–4, 10–20 February 2011, 318–327

Taylor & Francis
Taylor & Francis Group

Engineering an ideal indistinguishable photon-pair source for optical quantum information processing

Radhika Rangarajan[a]*, Luis Edgar Vicent[b], Alfred B. U'Ren[b] and Paul G. Kwiat[a]

[a]*Department of Physics, University of Illinois at Urbana-Champaign, 1110 W Green St., Urbana, IL 61801, USA;*
[b]*Instituto de Ciencias Nucleares, Universidad Nacional Autónoma de México, Apartado Postal 70–543, 04510 DF, Mexico City, Mexico*

(*Received 17 June 2010; final version received 2 August 2010*)

The eventual success of optical quantum information (QI) processing depends critically on the available technologies. Photons produced via the nonlinear process of spontaneous parametric downconversion (SPDC) have now been used in a vast array of experiments in optical quantum computing and long-distance quantum communication. However, almost no source to date has been fully optimized. Here, we describe our progress in engineering an ideal photon-pair source for optical quantum information processing – polarization-entangled photons made indistinguishable by engineering spatio-spectral *un*entanglement at the source. We present solutions for several key challenges encountered in the development of the indistinguishable source. We expect such a source to directly translate into significantly enhanced QI protocols with higher rates, fidelities and efficiencies.

Keywords: parametric downconversion; factorable state; source

1. Introduction

Two-photon interference manifests itself ubiquitously in linear optical quantum computing and quantum communication, in the form of the Hong-Ou-Mandel (HOM) interferometer [1]. For most quantum information (QI) applications, including teleportation, a HOM measurement must be performed between photons originating from different sources. Such an 'event-ready' HOM consists of two independent sources, each of which generates a photon pair; two photons, one from each source, are then combined at a beam-splitter. Here, mere indistinguishability between the two interfering photons does not suffice; any 'which-process' information carried by the non-interfering partner photons essentially makes the interfering processes distinguishable. Thus, indistinguishable photon-pair sources – photons uncorrelated in spatial-mode and frequency – are required for high-fidelity optical quantum information (QI) protocols [2]. Currently, nearly all experiments solve this problem by incorporating extremely narrow-band spatial and spectral filters to reduce any distinguishing information. However, filtering also drastically reduces the incident photon flux, thereby greatly lowering the overall efficiency. A better solution is to use unentangled photons [3–10], i.e. photons with no spatio-spectral correlations. Such truly indistinguishable photons would provide high-visibility interference without filtering. However, for useful QI processing we still need usable entanglement, another fundamental resource for QI, in at least one degree of freedom, e.g. polarization. Here, we describe our progress in engineering an ideal indistinguishable photon-pair source for optical QI processing – polarization-entangled photons with spatio-spectral *un*entanglement. We expect such a source to significantly improve the rates, efficiencies and fidelities of several QI protocols.

2. Engineering an indistinguishable-photon source

Our approach to developing an indistinguishable polarization-entangled photon pair source relies on spontaneous parametric downconversion (SPDC) and consists of two parts. First, we engineer unentanglement in the spatial mode and frequency between two photons generated from a single SPDC crystal, based on a group-velocity matching technique presented in [7]. Then we incorporate standard schemes – the two-crystal geometry [11–12] and the 'rail-cross' arrangement [13–15] – to generate polarization entanglement between different pairs of spatio-spectrally engineered photons.

*Corresponding author. Email: rangaraj@illinois.edu

ISSN 0950–0340 print/ISSN 1362–3044 online

DOI: 10.1080/09500340.2010.529515
http://www.informaworld.com

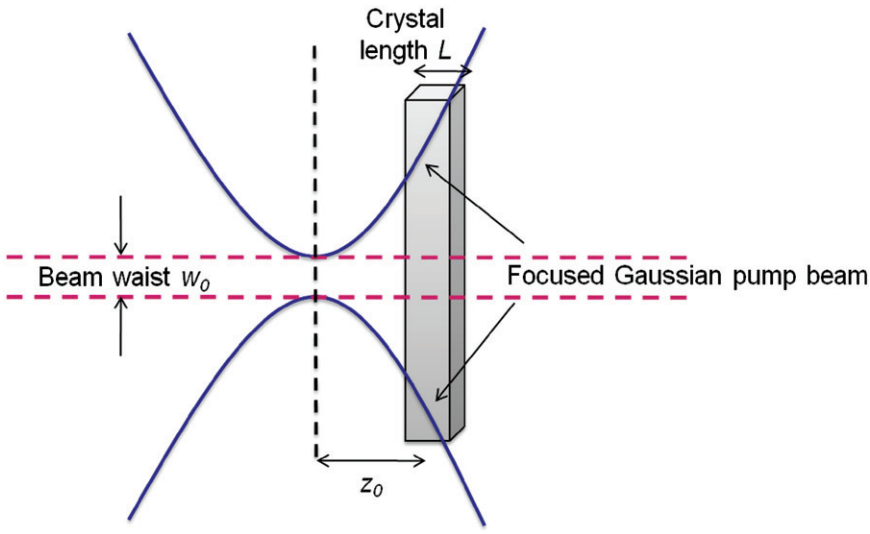

Figure 1. SPDC parameters – crystal length L, pump beam waist w_0, and position of beam waist z_0 measured relative to the crystal center. (The color version of this figure is included in the online version of the journal.)

2.1. *Eliminating spatial and spectral correlations in SPDC photons*

Our first step in engineering the indistinguishable-photon source consists of imposing group-velocity matching and optimizing the phasematching parameters for non-collinear, degenerate type-I SPDC to achieve maximum unentanglement in both frequency and spatial modes. The complete theory and the details behind the group-velocity matching technique to engineer the spatial and spectral characteristics of the downconversion photons can be found in [7]. In brief, the two-photon downconverted state can be written in terms of creation operators acting on the vacuum state as

$$|\Psi\rangle = \int d\mathbf{k}_s \int d\mathbf{k}_i \, f(\mathbf{k}_s, \mathbf{k}_i) \hat{a}_s^+(\mathbf{k}_s) \hat{a}_i^+(\mathbf{k}_i) |vac\rangle, \qquad (1)$$

where the subscripts s and i stand for signal and idler, respectively. $f(\mathbf{k}_s, \mathbf{k}_i)$, the joint two-photon amplitude (JPA) that characterizes the two-photon state, depends on the phase-matching conditions and SPDC parameters such as the crystal length L, pump beam waist w_0, position of beam waist z_0 and pump spectral bandwidth σ (see Figure 1). Figure 2(a) and (b) shows the typical source geometry, which defines the polar (θ) and azimuthal (ϕ) downconversion emission angles. In typical SPDC configurations, correlations can exist in and between the spectral (ω) and angular (both θ and ϕ) degrees of freedom of the downconversion beams. These correlations can be derived from the JPA, since $f(\mathbf{k}_s, \mathbf{k}_i)$ is a function of the wave vectors, which in turn depend on ω, θ and ϕ [7].

Figure 2(c) shows the different types of dominant correlations that typically exist between the signal and the idler photons for a type-I downconversion source pumped with a pulsed laser. External or inter-photon correlations exist between the signal and the idler photons, and are denoted by solid lines in Figure 2(c). These constitute azimuthal–azimuthal (e.g. photons are emitted on opposite sides of the pump beam as shown in Figure 2(c)), spectral–spectral, polar–polar and hybrid spectral-polar entanglement between the photons in a downconversion pair [7]. There are also internal or intra-photon correlations, denoted by the vertical dashed lines in Figure 2(c), between the frequency and polar emission angle of the same photon; such correlations, for example lower frequency components of the downconverted photons emerging at wider angles, can be thought of as being similar to a chirp in a classical field. Correlations involving azimuthal angles, on the one hand, and polar angles/frequencies, on the other hand, tend to be weak and are not shown in Figure 2(c).

For true indistinguishability, the JPA must be factorable in all photonic degrees of freedom (DOFs). The mechanism for tailoring the photon-pair entanglement properties relies on optimizing the source parameters, such as σ (by choosing a spectrally broad pump source), w_0 (by adjusting the pump beam focus), and L (by specifying the crystal length). Additionally, group velocity matching (along with the required phase matching) reduces most of the intra-photon and inter-photon correlations. Using the conditions derived by Vicent and colleagues [7], we can deduce the optimized specifications for generating frequency-degenerate

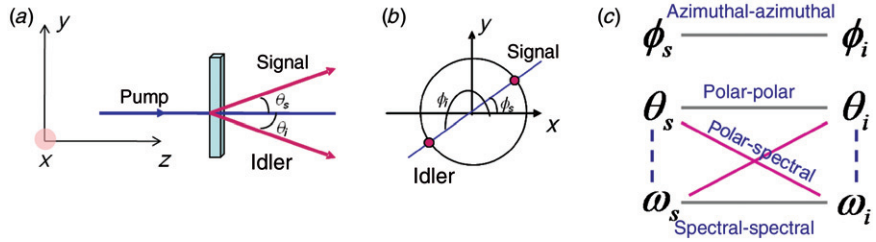

Figure 2. Basic SPDC source geometry. (*a*) Side view showing the emission polar angles. (*b*) Looking into the pump view, showing the emission azimuthal angles. (*c*) Dominant correlations between the signal and idler photons. (The color version of this figure is included in the online version of the journal.)

SPDC photon pairs, e.g. centered at 810 nm using a β-barium borate (BBO) crystal pumped by an ultrashort pulse train centered at 405 nm. The internal emission angle at which vector group-velocity matching occurs is $\theta_{s0} = -\theta_{i0} = 9/96^\circ$, which corresponds to $\sim 16^\circ$ external propagation angle. For this emission angle, and for the selected central emission frequency, the required crystal-cut angle required to attain phasematching is $\theta_{\rm pm} = 40.7^\circ$ (we also assume an azimuthal orientation of the optic axis of $\phi_{\rm pm} = 30^\circ$, for which the effective non-linearity is near its maximum). The optimal crystal length can be shown to be close to $L = 300\,\mu$m, based on the overlap of the downconversion modes from the crystal with the fiber-collection modes. Further, the required pump-beam radius is $w_{\rm o} = 23\,\mu$m (at $z_0 = 0$) and the pump bandwidth is ~ 28 nm at 405 nm. Such an optimization predicts greater than 90%-visibility HOM interference and a $\sim$900-fold improvement in the coupled brightness (compared with typical filtered geometries, for example see [16–21]). However, note that to create such a pump, we would have to frequency-double an ~ 80 nm bandwidth (~ 20 fs pulse width) Ti-sapphire laser; such large bandwidths are experimentally challenging to work with due to complications arising from dispersion, chirp, etc. Therefore, we initially use a quasi-optimized source: a 600-μm long BBO crystal that is group-velocity matched, requiring an optimized pump focus $w_{\rm o} = 46\,\mu$m and an optimized bandwidth at 405 nm of 15 nm (experimentally, we start with $\sigma = 4$ nm at 405 nm, generated using a doubled $\sim$90-fs Ti-sapphire laser). The quasi-optimized source is still expected to have a $\sim$230-fold improvement in the coupled brightness (compared with typical filtered geometries), with greater than 90% HOM interference visibilities.

A related application for these techniques is a heralded source of single photons: detection of one member of a pair heralds the presence of the other. Such a source may be further extended to prepare single photons on demand, as well as desirable multiphoton states; for example, number states and maximally entangled 'NOON' states [22]. One important factor of a useful heralded source is the heralding efficiency, defined as the probability of finding a photon in a definite state given the detection of its conjugate. Note that in order to produce any of the multiphoton states, it is again critical that the heralding and the heralded photon not be entangled with each other, i.e. as above, we need indistinguishable photons.

2.2. *Incorporating polarization entanglement*

Type-I polarization-entangled photons can be generated using the two-crystal geometry [11]: two adjacent thin nonlinear crystals are oriented orthogonally, such that a vertically V (horizontally H) polarized pump photon can downconvert into a pair of horizontally (vertically) polarized photons in the first (second) crystal. If the downconversion processes in each crystal are coherent with one another, pumping with photons polarized at 45° ideally generates a pure maximally entangled state:

$$|\psi\rangle = \frac{1}{\sqrt{2}}\left(|H_1 H_2\rangle + e^{i\phi(\omega_p,\omega_s,\omega_i,\mathbf{k}_p,\mathbf{k}_s,\mathbf{k}_i)}|V_1 V_2\rangle\right). \quad (2)$$

The relative phase ϕ in Equation (2) is determined by phasematching constraints and depends on various parameters such as crystal type and length, and pump (downconversion) frequency ω_p (ω_s, ω_i) and momentum vector $\mathbf{k}_p$ ($\mathbf{k}_s$, $\mathbf{k}_i$).

Typically, the source employs (only) phasematched crystals, and the SPDC parameters are not entirely optimized. By employing two group-velocity matched optimized SPDC crystals, which can each generate spatio-spectrally unentangled photons, we can, in principle, engineer a truly indistinguishable source. However, the integration of the spatio-spectral unentanglement techniques with the two-crystal scheme for producing polarization entanglement leads to at least three challenges: spectral-temporal decoherence,

emission-angle dependence of downconversion polarization (Migdall effect) and the need for birefringent focusing/collection.

3. Dominant challenges and their solutions

3.1. Spectral and spatial decoherence

One of the usual requirements to engineer indistinguishable photons is a broad bandwidth pump [7], realized by an ultrafast femtosecond laser; the wide range of frequencies relaxes the strict limitation imposed by energy conservation, resulting in minimal spectral correlations in the engineered source.[1] Thus, the pump bandwidth, along with the crystal length (which determines the range of pump frequencies that are phasematched for downconversion) need to be optimized to eliminate spectral correlations. However, decoherence in ultrafast entanglement sources causes a tradeoff between source brightness and fidelity,[2] making it challenging to create an efficient high-fidelity type-I polarization-entangled source using these pumps. In ultrafast pulsed two-crystal type-I sources, unlike sources with a monochromatic CW-pump, each frequency component of the broadband pump sees a different effective length of the crystal due to dispersion; averaging over the associated phases then leads to effective decoherence and reduced entanglement. Similarly, downconversion photons emitted at varying angles and frequencies can acquire different relative phases. Collecting multiple such states through large-diameter irises and large-bandwidth spectral filters results in averaging over the phases, leading to effective spatial decoherence [23]. Spectral decoherence can be countered by 'precompensating' the pump by passing it through a birefringent crystal before the downconversion crystals [24]. Spatial decoherence can be similarly eliminated by directing the downconversion photons through suitable birefringent compensating crystals that have the opposite phase characteristics as that of the downconversion crystals [25]. By effectively combining these temporal precompensation and spatial compensation techniques, we have demonstrated an extremely high-fidelity (>99%) ultrafast type-I polarization entanglement source [23] and overcome the first challenge imposed by a broad-bandwidth pump.

3.2. The Migdall effect

The second challenge arises because simultaneous group-velocity and phase-velocity matching in the engineered source results in a large (external) emission angle of 16°. As shown by Migdall [26], the polarizations of the downconverted photons vary with their emission angles, because the ordinary downconversion polarization must be perpendicular to the propagation direction and the crystal optic axis; further details on the theory can be found in [26]. As demonstrated in [27], the Migdall effect becomes appreciably larger for larger cone opening angles, with a 16° downconversion cone exhibiting up to a $\sim 12^\circ_p$ deviation[3] from the expected 90°_p polarization, compared with only a $\sim 3^\circ_p$ maximum deviation for a 3° cone.

The Migdall effect in the engineered two-crystal scheme has serious consequences on the generated entangled state; for the 16° downconversion cone, the emitted two-photon polarization state is $|\psi\rangle_{\text{migdall}} = (|78^\circ_p, 120^\circ_p\rangle + |0^\circ_p, 0^\circ_p\rangle)/\sqrt{2}$ (collected at 0° and 180° azimuthal angles for the first crystal, and 90° and 270° azimuthal angles for the second crystal) [27] and no longer the ideal maximally entangled state $|\psi\rangle_{\max} = (|90^\circ_p, 90^\circ_p\rangle + |0^\circ_p, 0^\circ_p\rangle)/\sqrt{2}$. Thus, the polarizations produced by the two crystals are no longer orthogonal to each other; more importantly, there is no basis in which they can be written as a maximally entangled state. The fidelity of $|\psi\rangle_{\text{migdall}}$ with $|\psi\rangle_{\max}$ is only 96%;[4] the predicted concurrence of $|\psi\rangle_{\text{migdall}}$ is 90.8%, if there were *no* temporal decoherence. Additionally, there is a significant component (~3%), quantified by the overlap between the downconversion states generated from the two crystals, that cannot be temporally compensated, and therefore experiences unavoidable decoherence. The final predicted maximum concurrence is ~88%.

As suggested in [27], we can exploit the Migdall effect to create a nearly maximally entangled state, by collecting at non-traditional azimuthal angles, i.e. locations where the relative polarizations between the downconversion photons generated from the two crystals are almost orthogonal. Such a strategy should maximize the overlap with the ideal maximally entangled state and produce, after local corrections, $(|93.4^\circ_p, 86.6^\circ_p\rangle + |0^\circ_p, 0^\circ_p\rangle)/\sqrt{2}$, which has >99% predicted fidelity with a maximally entangled state and a concurrence above 98%. Experimentally, however, while we do produce the states $|93.4^\circ_p, 86.6^\circ_p\rangle$ and $|0^\circ_p, 0^\circ_p\rangle$ from each of the respective crystals, by collecting at non-traditional angles, experimentally the resulting polarization-entangled state does not exhibit a high degree of polarization entanglement. The large 16° downconversion emission, combined with the unconventional collection angles, results in numerous other related issues, such as extreme sensitivity to temporal and spatial compensation. For example, the group-velocity matched crystals have an extremely large spatial-phase slope [23] of ~73°-per-mm compared with 15°-per-mm for the typical 3° downconversion propagation (at ~120 cm from the downconversion crystal). Thus, spatial decoherence alone theoretically limits the concurrence to ~66%

(compared to 98% for the 3° cone) when collecting through 2-mm irises. Collecting at the unconventional Migdall angles actually worsens spatial decoherence, with a ~78°-per-mm phase slope. This spatial decoherence can be countered using a 1.46-mm BBO compensator cut similar to the downconversion crystal [23]. However, such long crystals (the compensators are ~2.5 times the length of the SPDC crystals) can result in significant birefringent effects of their own, e.g. the total temporal walkoff (including the SPDC crystals) corresponds to ~535 fs, making this configuration extremely sensitive to temporal compensation. Experimentally, the highest concurrence obtained was only ~45%,[5] using the non-traditional collection angles suggested in [27] to overcome the Migdall effect. Possible sources of decoherence include polarization rotation in the SPDC crystal, spatial walkoff, dispersion, etc.

3.3. *Birefringent focusing*

The third challenge involved in engineering an indistinguishable photon-pair source – birefringent focusing – arises from the requirement to optimize phasematching parameters in our system. Figure 3 shows the effect of varying the focused pump beam-waist location z_0 (measured relative to the center of a single 0.6-mm group-velocity matched crystal) on the brightness and purity[6] of the single-mode fiber-coupled SPDC photons. We see that the pump beam has to be focused into the center of a crystal to generate bright spatially-spectrally unentangled photons. Thus, the pump beam-waist's size and location need to be optimized individually for each crystal (pumped with orthogonal polarizations), resulting in the need for birefringent focusing. Although the optimal pump beam waist size is the same for both polarizations (since our approach is simply to optimize downconversion from each of the crystals), one of the pump polarizations has to be focused one crystal length away, as shown in Figure 4. The inverse problem, birefringent collection, is similarly required since orthogonally-polarized downconversion photons, from the center of each crystal, have to be optimally collected into single-mode fibers.

3.4. *Experimental schemes for birefringent focusing*

The obvious approach to birefringent focusing might seem to be to employ a lens in combination with a birefringent slab to shift the focus of one of the polarizations. However, as discussed in [28] this technique actually fails to achieve the desired effect, i.e. two displaced round focused spots with orthogonal polarizations. When focusing using a lens and a

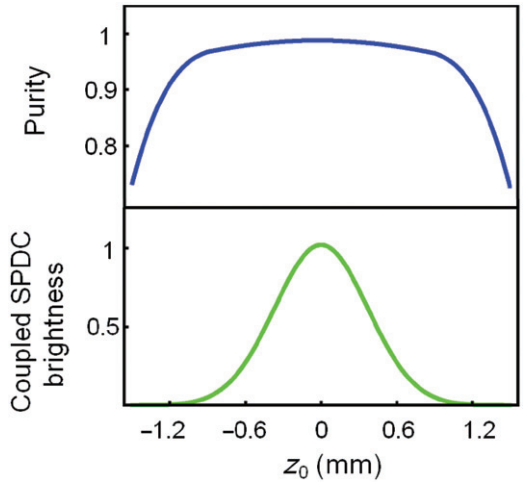

Figure 3. Simulated purity and normalized brightness dependence of the coupled SPDC photons on the position of the (focused) pump beam waist z_0, measured relative to the center of the crystal (assuming 0.6-mm group-velocity matched BBO crystals). (The color version of this figure is included in the online version of the journal.)

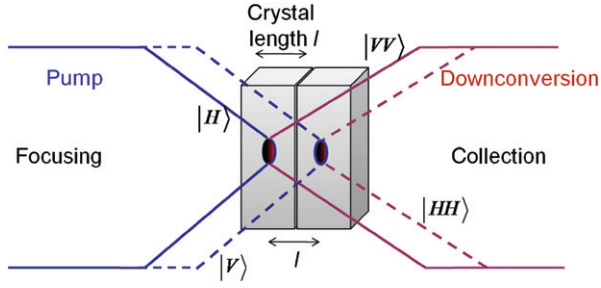

Figure 4. Schematic showing birefringent focusing (collection). The orthogonally polarized pump (downconversion) components, shown by solid and dashed lines, need to be focused at (collected from) the center of two different crystals, separating the beam waists of the different polarizations by one crystal length. (The color version of this figure is included in the online version of the journal.)

birefringent crystal, the ordinary polarized light behaves as expected, resulting in a longitudinal focus shift. However, the extraordinary polarized ray results in an elongated blurred focus, as extraordinary rays in different planes of incidence experience different longitudinal shifts because of the varying angle-dependent refractive indices inside the crystal [28].

Nevertheless, the underlying idea behind this method, having a polarization-dependent optical path length, can be implemented in other ways. For instance, one can use a lens followed by an unbalanced interferometer, e.g. a Mach–Zehnder, as shown in Figure 5(*a*). Here, a polarizing beam-splitter (PBS)

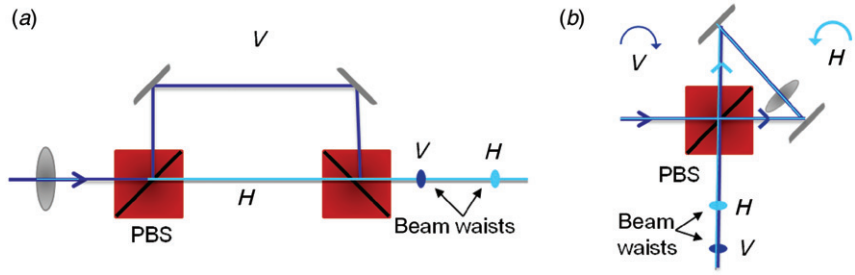

Figure 5. (*a*) A Mach–Zehnder-like setup to achieve birefringent focusing. A polarizing beam-splitter (PBS) is used to separate the two polarizations, and the foci separation is given by the path-length difference between the two arms. (*b*) A Sagnac-based implementation of birefringent focusing. A PBS is used to direct the orthogonal polarizations into clockwise and anti-clockwise paths. A focusing lens is placed offset from the center of the two paths. In the figure, the horizontal polarization sees the lens first, and thus is focused before the vertically polarized beam. (The color version of this figure is included in the online version of the journal.)

directs the different polarizations into different spatial arms, one longer than the other. The foci of the two different polarizations are thus controlled by the difference in the optical path lengths between the two arms. The disadvantage in using most interferometers, including the Mach–Zehnder, is that they are extremely sensitive to any path-length differences between the two arms; in order to preserve the coherence between the two arms (and the final relative phase ϕ between the $|HH\rangle$ and $|VV\rangle$ terms), they require interferometric stability at the sub-wavelength scale.

A more stable interferometer, the Sagnac (Figure 5(*b*)), circumvents the stability problem by using the same spatial path for the two arms. Here, the clockwise and counter-clockwise directions constitute the two arms. Thus, any noise becomes common-mode, making the interferometer extremely stable. Birefringent focusing can be achieved by placing a focusing lens displaced from the midpoint of the path. As shown in Figure 5(*b*), horizontally polarized light takes the counterclockwise path, sees the lens first and, hence, focuses before the vertical polarization. The distance between the two foci $\Delta f = 2x$, with x corresponding to the distance of the lens from the center. However, to engineer the indistinguishable source we need to optimize collection as well as focusing. Given that the downconversion beams are non-collinear, we would thus need to use three such Sagnac interferometers – one for the pump and one for each of the downconversion arms, substantially increasing the complexity of the source.

Alternatively, one might be able to use two spatially separated crystals with appropriate lenses, for optimal focusing of the differently polarized pumps, between the two crystals [29].

To evaluate the complications introduced by the three challenges in engineering the indistinguishable-photon polarization entangled source, let us list the proposed remedies: first, we need a temporal precompensator to eliminate spectral-temporal decoherence caused by an ultrashort femtosecond pump;[7] second, we collect at unconventional cone angles to reduce the Migdall effect; and finally, we should add three interferometers, e.g. Sagnacs, to optimize pump focus and downconversion collection. All of these steps are required, rather than simply inserting some narrow bandwidth filters – the conventional way of dealing with signal-idler correlations. Thus, while we have identified, understood and solved three challenges to engineering an indistinguishable-photon entanglement source, we are led to reconsider our overall approach. Most of the complications arise from incorporating these group-velocity matched engineered crystals in the two-crystal scheme for polarization entanglement. Thus, we can explore an alternate method – the 'rail-cross arrangement' – to generate polarization entanglement using the group-velocity matched SPDC crystals.

3.5. *The rail-cross arrangement*

The rail-cross scheme, shown in Figure 6, uses a single SPDC crystal and a double-pass pump arrangement to generate type-I polarization-entangled photons. The rail cross has been demonstrated with the typical $\sim 3^\circ$ SPDC emission angles [13,14]. Here, an extraordinary polarized pump, e.g. horizontally polarized, is incident on a downconversion crystal, with an amplitude to produce SPDC photons in the $|VV\rangle_1$ state. The pump is then reflected back through the crystal, with an amplitude to produce a pair in the $|VV\rangle_2$ state. The subscript on the downconversion state indicates the pump pass, i.e. first or second, that generated it. The $|VV\rangle_1$ spatial modes are also reflected back through the crystal, such that they overlap with the $|VV\rangle_2$

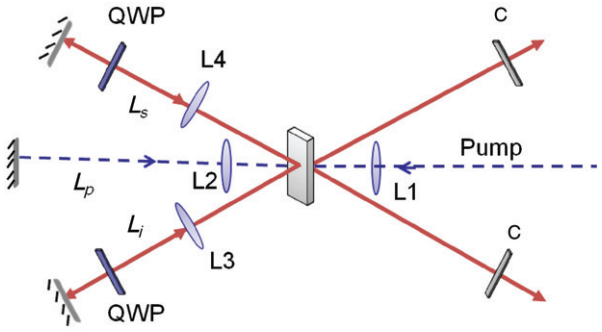

Figure 6. The rail-cross arrangement to generate type-I polarization-entangled photons (after [13]). Two downconversion paths are coherently superposed to produce the entangled state $|HH\rangle_1 + |VV\rangle_2$. The path lengths L_i, L_s, L_p are matched such that $|HH\rangle_1$ and $|VV\rangle_2$ exit the crystal at the same time. Compensators C in each downconversion arm compensate for the spatial (Poynting) walkoff. Lenses L1 and L2 are used to optimally focus the pump for both the passes and are located one focal length away from the center of the crystal. Lenses L3 and L4 are used to collimate the first-pass downconversion modes and refocus them back into the crystal, such that $|HH\rangle_1$ and $|VV\rangle_2$ can be optimally collected into single mode fibers. L3 and L4 are located one focal length away from the center of the crystal. (The color version of this figure is included in the online version of the journal.)

spatial modes [14]. However, the $|VV\rangle_1$ photons first pass through quarter-wave plates (QWP) in each arm, are reflected back and pass through the QWPs again; the wave plates are oriented such that after both these passes, $|VV\rangle_1$ becomes $|HH\rangle_1$. The optical path lengths L_s, L_i and L_p of the signal, idler and pump between the crystal and the respective mirrors are set so that the arrival times of all three are matched at the crystal. The downconversion states from both the pump passes are thus interferometrically combined; when they are coherent with each other,[8] they constitute the polarization-entangled state $|HH\rangle_1 + e^{i\Delta\phi}|VV\rangle_2$, where $\Delta\phi = \phi_s + \phi_i - \phi_p$, and ϕ_s, ϕ_i and ϕ_p denote the phases acquired by the signal, idler and pump in propagating to their respective mirrors and back, e.g. $\phi_p = 2\pi L_p/\lambda_p$. Note that interferometric stability between the first and second passes is a key requirement for high-fidelity polarization-entangled states, i.e. the path lengths L_s, L_i and L_p should be stable to within ~10 nm [15].

3.6. *Engineering an indistinguishable source with the rail cross*

The spatio-spectrally engineered crystal can be employed in a rail-cross arrangement to create an indistinguishable polarization-entangled photon-pair source. We can analyze the impact of the three main effects that complicated the two-crystal approach – temporal decoherence, the Migdall effect and birefringent focusing – in the rail cross arrangement. The first effect, temporal decoherence, can be accounted and compensated for using the methods discussed in [23]. The temporal delay Δt between $|HH\rangle_1$ and $|VV\rangle_2$ is the overall difference in the arrival times between the downconversion states generated from the first and second pump passes.[9] When $L_s = L_i$, the walkoff t^{HH} and t^{VV}, of $|HH\rangle_1$ and $|VV\rangle_2$, respectively, relative to the pump can be written in terms of the crystal length L, the propagation times (inside the crystal) of the horizontally polarized pump t_H^p, and the vertically and horizontally polarized downconversion states, t_V^{dc} and t_H^{dc}, respectively, as:

$$t^{HH} = t_V^{dc}(l/2) + 2\frac{L_s}{c} + t_H^{dc}(l) \tag{3}$$

$$t^{VV} = t_H^p(l/2) + 2\frac{L_p}{c} = t_H^p(l/2) + t_V^{dc}(l/2) \tag{4}$$

$$\Delta t = t^{VV} - t^{HH} = t_H^p(l) + 2\frac{L_p}{c} - 2\frac{L_s}{c} - t_H^{dc}(l). \tag{5}$$

The path lengths L_s, L_i and L_p can be matched[10] such that $|HH\rangle_1$ and $|VV\rangle_2$ are perfectly temporally compensated ($\Delta t = 0$). Alternatively, instead of tweaking L_s, L_i and L_p to control the temporal walkoff, another birefringent crystal could be used to compensate for this delay. Thus, spatial and temporal compensators can be designed using calculations similar to those in [23].

Additionally, *spatial walkoff* (Poynting vector walkoff) needs to be accounted for in the engineered double-pass scheme.[11] Spatial walkoff would result in only a partial spatial overlap of $|HH\rangle_1$ and $|VV\rangle_2$. The amount of spatial walkoff ρ can be given in terms of the optic axis cut angle θ, and extraordinary and ordinary indices of refraction n_e and n_o, respectively, by [30]:

$$\rho = \theta - \arctan\left[\left(\frac{n_o}{n_e}\right)^2 \tan\theta\right]\mathrm{sgn}(n_o - n_e). \tag{6}$$

For an engineered crystal, $\rho = 4.3$ for the pump ($\rho = 4.1$ for the downconversion) corresponding to a transverse walkoff of ~46 μm (~43 μm) in a 0.6-mm crystal. Figure 7(*a*) and (*b*) shows a simplified schematic of the spatial walkoff of the various beams for each pass. Birefringent compensators C that are identical to the SPDC crystal,[12] placed in each of the second-pass downconversion arms (Figure 7(*c*)) completely compensate for the spatial walkoff that otherwise results in only partial spatial-mode overlap between $|HH\rangle_1$ and $|VV\rangle_2$. The spatial walkoff compensators can be easily

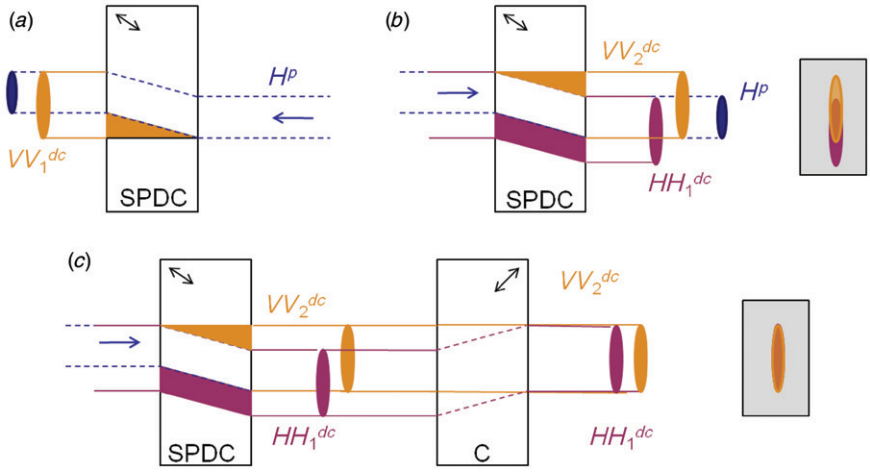

Figure 7. Poynting-vector walkoff and compensation in the rail-cross arrangement. (*a*) The extraordinary pump (blue) walks off during the first pass. The generated downconversion states $|VV\rangle_1$ (orange) are ordinary polarized and thus do not walk off; however, they are created along the entire length of the crystal, leading to an elliptical spot after the crystal. (*b*) After reflection and rotation by the quarter-wave plates, the first-pass downconversion photons $|HH\rangle_1$ (purple) are extraordinary polarized and, consequently, now exhibit walk off along with the pump (although to a slightly lesser degree due to the different refractive indices at the longer wavelengths). The second-pass downconversion photons $|VV\rangle_2$ (orange), however, do not exhibit walkoff, although again they are elliptical spots after the crystal. Thus, there is only a partial spatial overlap (~50% for 0.6-mm GVM SPDC crystals). (*c*) The Poynting-vector walkoff can be compensated using a birefringent element C identical to the SDPC crystal to obtain complete spatial overlap.[14] The double-sided arrows (black) indicate the optic axis orientation in the SPDC and compensator crystals. (The color version of this figure is included in the online version of the journal.)

designed using Equation (5). Note that the temporal walkoff in the compensators themselves have to be accounted for and can be compensated by adjusting the appropriate path lengths.[13]

The second main effect, the directional dependence of the downconversion polarization – the Migdall effect – ceases to be a problem when we employ the rail-cross arrangement for polarization entanglement. At the chosen wavelengths 405 nm → 810 nm + 810 nm the large 16° downconversion cone emission angle is still required for group-velocity matching in the engineered (BBO) crystal. However, since the downconversion occurs only in one crystal and always with the same polarization, e.g. $|H\rangle \rightarrow |VV\rangle$, the azimuthal collection angles can be chosen such that the downconversion polarization is perpendicular to that of the pump in the lab frame, i.e. we can always collect at the 90° and 270° points on the emission cone [26,27] where there is no Migdall effect.

The need for the third requirement, birefringent focusing is also eliminated. The engineering scheme calls for optimizing the pump beam waist. However, because the pump is always the same polarization in both the passes, birefringent focusing is unnecessary. The pump can be focused at the center of the crystal, for both passes, using a simple combination of two lenses, as shown in Figure 6. Lens L1 focuses the pump at the center of the crystal during the first pass and lens L2 collimates the beam on its first pass; the mirror reflects the pump back through L2, which now focuses the pump back at the center of the crystal. Similarly, birefringent collection is no longer needed. Lenses L3 and L4 are used to collimate the first-pass downconversion modes and, upon reflection by their respective mirrors, refocus them back into the crystal. L1, L2, L3 and L4 are all located one focal length away from the center of the crystal. The downconversion photons, in spite of the different polarizations, can be optimally collected by simple lenses in each arm because both $|HH\rangle_1$ and $|VV\rangle_2$ originate in the same crystal.

Thus, the rail-cross arrangement appears to be superior to the two-crystal scheme for engineering indistinguishable photons, specifically because it eliminates two of the three main challenges. Temporal compensation is still needed, but can be easily employed in the rail-cross scheme without any additional compensators. Admittedly, there are known challenges with the rail-cross arrangement that are not present with the two-crystal scheme, the biggest being the need for interferometric stability. Thus, although there might be new, unexpected challenges that complicate the rail-cross arrangement, it promises to be a viable route to engineering an ideal indistinguishable entanglement source for optical QI protocols.

4. Conclusions

In conclusion, we have discussed two approaches to realize an indistinguishable source using spatio-spectrally unentangled photons from group-velocity matched SPDC crystals: the two-crystal and the interferometric rail-cross arrangement for generating polarization entanglement. The deciding factors for the best route to the indistinguishable source are heralding efficiencies, and the tradeoff between the various experimental challenges analyzed here, including temporal/spatial decoherence, emission-angle dependence of the downconversion polarization, optimized focusing/collection and spatial walkoff. Currently, the engineered group-velocity matched crystal employed in a rail-cross arrangement appears to the most promising option. However, the optimization of a typical SPDC source using the approach presented here might be limited (either fundamentally or because of experimental challenges), in which case other engineering options, such as crystal superlattices [31], four-wave mixing in micro-structured fibers [3] etc., could be pursued.

Acknowledgements

This work was supported by the National Science Foundation (Grant No. EIA-0121568), MURI Center for Photonic Quantum Information Systems (ARO/ARDA Program DAAD19-03-1-0199), and the IARPA-funded Quantum Computing Concept Maturation Optical Quantum Computing Project (Contract No. W911NF-05-0397). AU also acknowledges support from CONACYT, Mexico, from DGAPA, UNAM and from FONCICYT Project 94142.

Notes

1. In contrast, using a CW pump leads to maximal spectral (anti-)correlation, since $\omega_s = \omega_p - \omega_i$.
2. Fidelity measures the amount of overlap between two states ρ_1 and ρ_2 $F(\rho_1, \rho_2) = (Tr\{\sqrt{\sqrt{\rho_1}\rho_2\sqrt{\rho_1}}\})^2$ which simplifies to $\left|\langle\psi_1|\psi_2\rangle\right|^2$ for pure states [23].
3. The subscript p indicates a polarization angle (defined with respect to the pump polarization in the SPDC crystal under consideration), as opposed to an emission angle.
4. In comparison, in the typical 3° half-opening angle geometry, the emitted state due to the Migdall effect is $|\psi\rangle_{\text{typical}} = (|93.2^\circ_p, 86.9^\circ_p\rangle + |0^\circ_p, 0^\circ_p\rangle)/\sqrt{2}$, which has a ~99.7% fidelity with the ideal state, sufficient for most applications to date.
5. We did not use any spatial compensators; instead, spatial-phase coherence was controlled by collecting with very small irises (<0.5 mm), at the expense of low rates and long collection times.
6. The single-photon purity (signal or idler) is defined as $Tr(\rho^2)$, where ρ is the density operator for the single mode obtained by tracing over the idler mode.
7. Spatial compensation is not of much help when coupling into single-mode fibers, which, at least initially, is required to confirm the theory of the engineered indistinguishable source.
8. The pairs from the first and second passes will be indistinguishable if $L_s - L_i \ll L_s^c = L_i^c$, i.e. the path lengths of the signal and the idler should be well within the coherence lengths of the downconversion photons L_c, and if $L_p - L_s \approx L_p - L_i < L_p^c$, i.e. the path length of the pump should be small compared to its coherence length L_p^c. Note that in the retro-reflection geometry the path lengths L_s, L_i and L_p correspond to twice the distance between the crystal and the corresponding mirrors.
9. The downconversion photons are assumed to be born in the center of the parent crystal.
10. For example, a temporal delay of 100 fs corresponds to ~33 μm path length in free space.
11. Spatial walkoff becomes significant in the engineered crystals mostly because of the pump beam waist optimization requirement. For 0.6-mm crystals, the optimized pump beam waist is ~45 μm. Spatial walkoff would complicate the original two-crystal scheme in the non-traditional Migdall-collection-angle scheme as well.
12. The compensation crystals are chosen to be identical to the SPDC for convenience. A number of other choices exist by making a tradeoff between optic-axis angle and thickness [27].
13. Collection using single-mode fibers obviates the need for any *spatial-phase* compensators, which would otherwise be required for free-space collection.
14. We have neglected the fact that the downconversion amplitude is coherently enhanced as the beams propagate through the crystals (~stimulated downconversion), which may lead the output ellipses to have a non-uniform probability density (e.g. lower at the top and the bottom of the ellipse). This effect would affect the calculated overlap somewhat.

References

[1] Hong, C.K.; Ou, Z.Y.; Mandel, L. *Phys. Rev. Lett.* **1987,** *59,* 2044–2046.
[2] U'Ren, A.; Banaszek, K.; Walmsley, I. *J Quantum Inf. Comput.* **2003,** *3,* 480–502.
[3] Cohen, O.; Lundeen, J.S.; Smith, B.J.; Puentes, G.; Mosley, P.J.; Walmsley, I.A. *Phys. Rev. Lett.* **2009,** *102,* 123603–123604.
[4] Kuzucu, O.; Fiorentino, M.; Albota, M.A.; Wong, F.N.C.; Kärtner, F.X. *Phys. Rev. Lett.* **2005,** *94,* 083601.
[5] U'Ren, A.B.; Silberhorn, C.; Banaszek, K.; Walmsley, I.A.; Erdmann, R.; Grice, W.P.; Rayme, M.G. *Laser Phys.* **2005,** *15,* 146–161.
[6] Valencia, A.; Cere, A.; Shi, X.; Molina-Terriza, G.; Torres, J.P. *Phys. Rev. Lett.* **2007,** *99,* 243601–243604.
[7] Vicent, L.E.; U'Ren, A.B.; Rangarajan, R.; Osorio, C.I.; Torres, J.P.; Zhang, L.; Walmsley, I.A. *New J. Phys.* **2010,** *12,* 093027.
[8] Brańczyk, A.M.; Ralph, T.C.; Helwig, W.; Silberhorn, C. *New J. Phys.* **2010,** *12,* 063001.

[9] Laiho, K.; Cassemiro, K.N.; Silberhorn, C. *Opt. Express* **2009,** *17,* 22823–22837.
[10] Shi, X.; Valencia, A.; Hendrych, M.; Torres, J.P. *Opt. Lett.* **2008,** *33,* 875–877.
[11] Kwiat, P.G.; Waks, E.; White, A.G.; Appelbaum, I.; Eberhard, P.H. *Phys. Rev. A* **1999,** *60,* R773–R776.
[12] Hardy, L. *Phys. Lett. A* **1992,** *161,* 326–328.
[13] Herzog, T.J.; Kwiat, P.G.; Weinfurter, H.; Zeilinger, A. *Phys. Rev. Lett.* **1995,** *75,* 3034–3037.
[14] Herzog, T.J.; Rarity, J.G.; Weinfurter, H.; Zeilinger, A. *Phys. Rev. Lett.* **1994,** *72,* 629–632.
[15] Lamas-Linares, A.; Howell, J.C.; Bouwmeester, D. *Nature* **2001,** *412,* 887–890.
[16] Bouwmeester, D.; Pan, J.W.; Daniell, M.; Weinfurter, H.; Zeilinger, A. *Phys. Rev. Lett.* **1999,** *82,* 1345–1349.
[17] Eibl, G.S.; Bourennane, M.; Kurtsiefer, C.; Żukowski, M.; Weinfurter, H. *Phys. Rev. Lett.* **2003,** *90,* 200403.
[18] Lu, Z.X.Q.; Guhne, C.Y.; Gao, O.; Zhang, W.B.; Zhang., J.; Yuan., Z.S.; Goebel, A.; Yang, T.; Pan, J.W. *Nat. Phys.* **2007,** *3,* 91–95.
[19] Pan, J.-W.; Daniell, M.; Gasparoni, S.; Weihs, G.; Zeilinger, A. *Phys. Rev. Lett.* **2001,** *86,* 4435–4438.
[20] Zhao, Z.; Chen, Y.-A.; Zhang, A.N.; Yang, T.; Briegel, H.J.; Pan, J.W. *Nature* **2004,** *430,* 54–58.
[21] Zhao, Z.; Chen, Y.A.; Zhang, A.N.; Zukowski, M.; Pan, J.W. *Phys. Rev. Lett.* **2003,** *91,* 180401.
[22] McCusker, K.T.; Kwiat, P.G. *Phys. Rev. Lett.* **2009,** *103,* 163602.
[23] Rangarajan, R.; Goggin, M.; Kwiat, P. *Opt. Express* **2009,** *17,* 18920–18933.
[24] Nambu, Y.; Usami, K.; Tsuda, Y.; Matsumoto, K.; Nakamura, K. *Phys. Rev. A* **2002,** *66,* 033816.
[25] Altepeter, J.; Jeffrey, E.; Kwiat, P. *Opt. Express* **2005,** *13,* 8951–8959; Erratum: Akselrod, G.M.; Altepeter, J.B.; Jeffrey, E.R.; Kwiat, P.G. *Opt. Express* **2007,** *15,* 5260–5261.
[26] Migdall, A. *J. Opt. Soc. Am. B* **1997,** *14,* 1093–1098.
[27] Rangarajan, R.; U'Ren, A.B.; Kwiat, P.G. *J. Mod. Opt.* **2011**, *58*, 312–317.
[28] Park, J.-H.; Jung, S.; Choi, H.; Lee, B. *Opt. Express* **2003,** *11,* 1862–1875.
[29] Brida, G.; Genovese, M.; Novero, C.; Predazzi, E. *Phys. Lett. A* **2000,** *268,* 12–16.
[30] Gurzadian, G.G.; Dmitriev, V.G.; Nikogosian, D.N. In *Springer Series in Optical Sciences*: Dmitriev, V.G., Gurzadyan, G.G., Nikogosyan, D.N., Eds.; Springer-Verlag: Berlin, New York, 1991; Vol. 64.
[31] U'Ren, A.B.; Erdmann, R.K.; de la Cruz-Gutierrez, M.; Walmsley, I.A. *Phys. Rev. Lett.* **2006,** *97,* 223602.